Search for axions from the Kuo-Sheng nuclear power reactor with a high-purity germanium detector

H. M. Chang,[1,2] H. T. Wong,[1,*] M. H. Chou,[1] M. Deniz,[1,3] H. X. Huang,[1,4] F. S. Lee,[1] H. B. Li,[1] J. Li,[5,6] H. Y. Liao,[1,2] S. T. Lin,[1,2] V. Singh,[1] S. C. Wu,[1] and B. Xin[4]

(TEXONO Collaboration)

[1]*Institute of Physics, Academia Sinica, Taipei 115, Taiwan*
[2]*Department of Physics, National Taiwan University, Taipei 106, Taiwan*
[3]*Department of Physics, Middle East Technical University, Ankara 06531, Turkey*
[4]*Department of Nuclear Physics, Institute of Atomic Energy, Beijing 102413, China*
[5]*Institute of High Energy Physics, Chinese Academy of Science, Beijing 100039, China*
[6]*Department of Engineering Physics, Tsing Hua University, Beijing 100084, China*

(Received 29 August 2006; revised manuscript received 24 October 2006; published 30 March 2007)

A search of axions produced in nuclear transitions was performed at the Kuo-Sheng Nuclear Power Station with a high-purity germanium detector of mass 1.06 kg at a distance of 28 m from the 2.9 GW reactor core. The expected experimental signatures were monoenergetic lines produced by their Primakoff or Compton conversions at the detector. Based on 459.0/96.3 days of reactor ON/OFF data, no evidence of axion emissions were observed and constraints on the couplings $g_{a\gamma\gamma}$ and g_{aee} versus axion mass m_a within the framework of invisible axion models were placed. The KSVZ and DFSZ models can be excluded for 10^4 eV $\lesssim m_a \lesssim 10^6$ eV. Model-independent constraints on $g_{a\gamma\gamma} \cdot g^1_{aNN} < 7.7 \times 10^{-9}$ GeV^{-2} for $m_a \lesssim 10^5$ eV and $g_{aee} \cdot g^1_{aNN} < 1.3 \times 10^{-10}$ for $m_a \lesssim 10^6$ eV at 90% confidence level were derived. This experimental approach provides a unique probe for axion mass at the keV-MeV range not accessible to the other techniques.

DOI: 10.1103/PhysRevD.75.052004 PACS numbers: 14.80.Mz, 29.40.−n, 28.41.−i

I. INTRODUCTION

The axions (a) [1] were proposed in the 1970s as a solution to the strong CP problem—the near-perfect cancellations between the QCD vacuum angle and the quark mass matrix, as constrained by experimental bounds on the neutron electric dipole moments. The interactions of the axions with matter (photons, electrons, and nucleons) can be described by the effective Lagrangian [1,2]

$$\mathcal{L}_{\text{int}} = g_{a\gamma\gamma}\phi_a \vec{E}\cdot\vec{B} + ig_{aee}\phi_a\bar{\psi}_e\gamma_5\psi_e + i\phi_a\bar{\psi}_N\gamma_5(g^0_{aNN} + g^1_{aNN}\tau_3)\psi_N, \quad (1)$$

where ϕ_a, $(\vec{E}, \vec{B})$, ψ_e, and

$$\psi_N = \begin{pmatrix} p \\ n \end{pmatrix}$$

represent, respectively, the axion, electromagnetic, electron, and nucleon fields. The couplings of the axions to the photons and electrons are parametrized by $g_{a\gamma\gamma}$ and g_{aee}, while g^0_{aNN} and g^1_{aNN} are their isoscalar and isovector couplings to the nucleons.

A generic feature of the axion models is that all the coupling constants as well as the axion mass (m_a) are inversely proportional to the symmetry breaking scale (f_a). The original Peccei-Quinn-Weinberg-Wilczek (PQWW) model [3] took f_a to be the electroweak scale, implying m_a of the order of ~100 keV. This has been tested and excluded after extensive efforts. Current research programs [4] focus on larger f_a in the "invisible axion models," the two popular variants of which are the DFSZ (or grand unified theory) [5] and KSVZ (or hadronic) models [6]. The axion couplings with matter within the framework of these models were evaluated and discussed in detail in Refs. [7,8].

The light-mass axion is a well-motivated dark matter candidate. Cosmological and astrophysical arguments [1,9] constrain the axion mass to be 10^{-6} eV $< m_a < 10^{-2}$ eV, but the bounds are model dependent and with large uncertainties. Experiments have been performed to look for dark matter axions as well as those produced in the Sun, power reactors, and radioactive nuclear transitions.

All previous reactor experiments [10,11] focused on the searches of the PQWW axions via their decays, and contributed much to exclude their existence. In this article, we present results on a new search over a broad axion mass range, using an alternative detection strategy through its interactions with matter. This detection scheme was successfully used in a previous experiment using a radioactive isotope as an axion source [2].

II. REACTOR AS AN AXION SOURCE

The axions are pseudoscalar particles and have quantum numbers like those of magnetic photons. It can be emitted

*Corresponding author
Electronic address: htwong@phys.sinica.edu.tw

through magnetic transitions in radioactive gamma decays [12]. Nuclear power reactors are powerful radioactive sources and are therefore potential axion sources as well. Axions can be emitted in competition with the photons as a result of neutron captures

$$n + (Z, A) \rightarrow (Z, A + 1) + \gamma/a \tag{2}$$

or nuclear deexcitations

$$(Z, A)^* \rightarrow (Z, A) + \gamma/a. \tag{3}$$

There are six prominent channels of magnetic gamma-transitions at typical nuclear reactors, as listed in Table I. Thermal neutron captures on the ^{10}B in the control rods and on the proton in the cooling water produce $\alpha + {}^7\mathrm{Li}^*$ and $d + \gamma$, respectively. Their photon fluxes (Φ_γ), in units of fission^{-1} and GCi, were evaluated by full neutron transport simulations [13]. The other sources of $^{91}\mathrm{Y}^*$, $^{97}\mathrm{Nb}^*$, $^{135}\mathrm{Xe}^*$, and $^{137}\mathrm{Ba}^*$ are all fission daughters. Their corresponding Φ_γ were derived from standard tables on fission yields [14] and cross checked by previous calculations [10]. For comparisons, the $\bar{\nu}_e$ [15] and ν_e yields [13] at reactors are about 7.2 and $\sim 10^{-3}$ fission^{-1}, respectively.

The axion flux (ϕ_a) at a distance L from a reactor core of fission rate R_f can be described by

$$\phi_a(L) = \frac{R_f \cdot \Phi_\gamma}{4\pi L^2} \cdot \frac{\Gamma_a}{\Gamma_\gamma} \cdot P_{dk} \cdot P_{\mathrm{int}}, \tag{4}$$

where (Γ_a/Γ_γ) is the branching ratio of axion emissions in the transitions. It depends on the axion-nucleon couplings and the nuclear structures of the transitions. The probabilities of the axions surviving the flight from reactor core to detector without decays or interactions are given, respectively, by

$$P_{dk} = \exp\left[-\frac{L \cdot m_a}{p_a \cdot \tau_a}\right] \tag{5}$$

and

$$P_{\mathrm{int}} = \exp[-L \cdot \rho_L \cdot \sigma_{\mathrm{int}}], \tag{6}$$

where m_a, τ_a, p_a, E_a are the axion mass, lifetime, momentum, and total energy; σ_{int} is the axion interaction cross section with matter at effective target number density ρ_L.

In particular, the axions can decay in flight via the emissions of 2γ ($\Gamma_{\gamma\gamma}$:$a \rightarrow \gamma\gamma$) or e^+e^- pairs (Γ_{ee}:$a \rightarrow e^+e^-$). Their decay rates are related to the $g_{a\gamma\gamma}$ and g_{aee} couplings by [12]:

$$\frac{1}{\Gamma_{\gamma\gamma}} = \frac{64\pi}{g_{a\gamma\gamma}^2 m_a^3} \tag{7}$$

and

$$\frac{1}{\Gamma_{ee}} = \frac{8\pi}{g_{aee}^2 \sqrt{m_a^2 - 4m_e^2}}. \tag{8}$$

The axion lifetime is then given by

$$\tau_a = \frac{1}{\Gamma_{\gamma\gamma} + \Gamma_{ee}}. \tag{9}$$

TABLE I. A summary of magnetic transitions and their estimated fluxes at a typical 2.9 GW power reactor.

Channel	E_γ (keV)	Transitions	Φ_γ (fission^{-1})	(GCi)
p(n, γ)d	2230	Isovector M1	0.25	0.61
^{10}B(n, α)^{7}Li*	478	M1($\frac{1^-}{2}$) $\rightarrow$ ($\frac{3^-}{2}$)	0.28	0.68
^{91}Y*	555	M4($\frac{9^+}{2}$) $\rightarrow$ ($\frac{1^-}{2}$)	0.024	0.058
^{97}Nb*	743	M4($\frac{1^-}{2}$) $\rightarrow$ ($\frac{9^+}{2}$)	0.055	0.13
^{135}Xe*	526	M4($\frac{11^-}{2}$) $\rightarrow$ ($\frac{3^+}{2}$)	0.0097	0.023
^{137}Ba*	662	M4($\frac{11^-}{2}$) $\rightarrow$ ($\frac{3^+}{2}$)	0.0042	0.010

III. AXION DETECTION AND EXPERIMENTAL SETUP

Data were taken with a high-purity germanium detector (HPGe) of mass 1.06 kg at the Kuo-Sheng (KS) Reactor Laboratory. The HPGe target and the associated anti-Compton (AC) detectors as well as passive shieldings are depicted in Fig. 1. The principal AC detector was a well-shaped NaI(Tl) crystal scintillator of mass 19.7 kg. Descriptions of the experimental hardware and analysis procedures were presented in detail in Refs. [15,16]. The primary scientific goal was the search of neutrino magnetic moments. A physics threshold of 12 keV and a background level of 1 day^{-1} kg^{-1} keV^{-1} comparable to those of underground dark matter experiments were achieved. The source-detector distance of KS was $L = 28$ m while ρ_L was modeled to be 27.75 m of water and 0.25 m of lead.

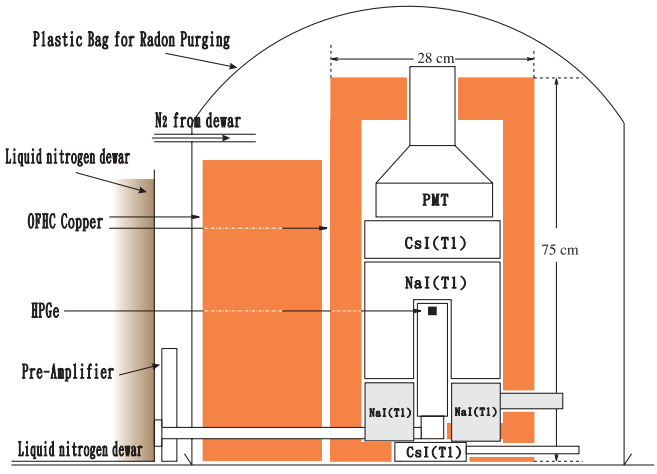

FIG. 1 (color online). Schematic layout of the HPGe with its anti-Compton detectors as well as inner shieldings and radon purge system.

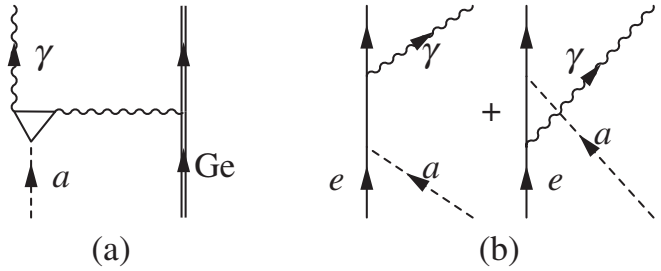

FIG. 2. Schematic diagrams of interactions of axions with matter, via (a) Primakoff and (b) Compton conversions.

The search strategies for reactor axions with these unique HPGe data were inspired by a previous experiment [2] where a 15 kCi γ-source of ^{65}Zn was used as a potential axion source instead. Two interaction mechanisms of axions with matter were studied: Primakoff and Compton conversions as shown schematically in Figs. 2(a) and 2(b). These processes are, respectively, and independently sensitive to $g_{a\gamma\gamma}$ and g_{aee}. Their cross sections were both given in Ref. [2]—(a) Primakoff conversion on the nuclei:

$$\sigma_P = g_{a\gamma\gamma}^2 \frac{Z^2 \alpha_{\rm em}}{2} \frac{1}{\beta}\left[\frac{1+\beta^2}{2\beta}\ln\left[\frac{1+\beta}{1-\beta}\right]-1\right]\chi, \quad (10)$$

where $\alpha_{\rm em}$ is the electromagnetic coupling, Z is the atomic number of the target, $\beta = p_a/E_a$ and χ is the atomic-screening correction factor given in Eq. (20) of Ref. [2]; (b) Compton conversion on the electrons:

$$\sigma_C = g_{aee}^2 \frac{\pi \alpha_{\rm em}}{8\pi m_e^2 p_a}\left[\frac{2m_e^2(m_e+E_a)y}{(m_e^2+y)^2} + \frac{4m_e(m_a^4+2m_a^2m_e^2-4m_e^2E_a^2)}{y(m_e^2+y)} + \frac{4m_e^2p_a^2+m_a^4}{p_a y}\ln\frac{m_e+E_a+p_a}{m_e+E_a-p_a}\right], \quad (11)$$

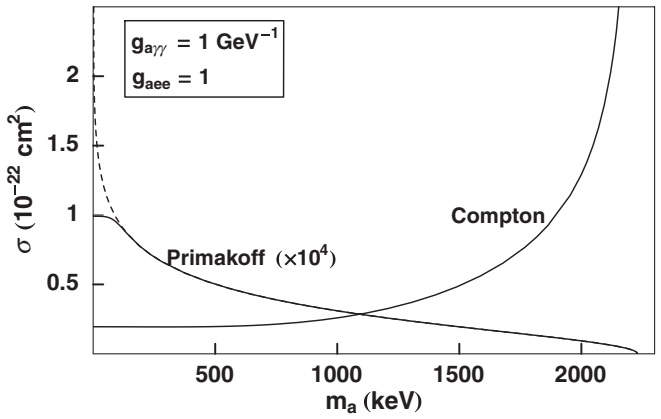

FIG. 3. The variations of the Primakoff and Compton conversion cross sections with the axion mass at $E_a = 2.23$ MeV, using the normalizations of $g_{a\gamma\gamma} = 1$ GeV^{-1} and $g_{aee} = 1$. The dashed line represents the case where the atomic-screening effects are switched off ($\chi = 1$).

where $y = 2m_eE_a + m_a^2$. The m_a dependence of the two cross sections at the pn $\rightarrow$ dγ transition energy of $E_a = 2.23$ MeV, using the normalizations of $g_{a\gamma\gamma} = 1$ GeV^{-1} and $g_{aee} = 1$, are illustrated in Fig. 3.

The total energy of the axions can be fully converted by either of the two processes into measurable ionization energy in the HPGe, such that the experimental signatures are the presence of monoenergetic lines at the known E_a's during the reactor ON periods. In comparison, previous reactor-based axion experiments studied instead the axion decay channels $\Gamma_{\gamma\gamma}$ [10] or Γ_{ee} [11]. They were therefore not sensitive to the invisible axion regime where m_a are very small and decays are kinematically blocked or suppressed.

IV. DATA ANALYSIS

The signal rates ($S_{P/C}$) for axion Primakoff/Compton conversions in 1 kg of target mass are given by

$$S_P = \sigma_P \cdot \phi_a \cdot N \cdot \epsilon_P \quad (12)$$

and

$$S_C = \sigma_C \cdot \phi_a \cdot Z \cdot N \cdot \epsilon_C, \quad (13)$$

where $\epsilon_{P/C}$ are the efficiencies of full-energy deposition at the HPGe detector, N is the number of atoms in the kilogram target, and Z accounts for the electron target number in the Compton process. The various efficiency factors were evaluated by full simulations and listed in Table II. Full-energy depositions for Compton conversion at the HPGe detectors were due to interactions only in Ge, such that only N(Ge), Z(Ge) = 32, and ϵ_C(Ge) were involved in the derivation of S_C. However, photons from Primakoff conversions in both Ge and NaI could contribute to S_P as full-energy peaks at the HPGe, such that there are terms involving, respectively, [N(Ge), ϵ_P(Ge)] and [N(NaI), ϵ_P(NaI)].

Evidence of reactor axions would manifest as peaks at the known energies of Table I in the reactor ON-OFF residual spectra in HPGe. Following the naming conventions of Ref. [15], Period I (July 2001–April 2002) and Period III (Sept. 2004–Oct. 2005) with 180.1/52.7 and 278.9/43.6 days of the KS-HPGe reactor ON/OFF data, respectively, were used for the analysis. Candidate events were those uncorrelated with the anti-Compton and cosmic-ray vetos and having pulse shapes consistent with γ-events. Selections of these events and their efficiencies were discussed in Ref. [15]. As illustrations, the Period III ON/OFF background spectra and the ON-OFF residual spectra for the six candidate lines are depicted in Figs. 4(a) and 4(b), respectively. The background γ-lines were identified [15] and indicated that ambient radioactivity dominated.

The count rates and their errors of the various transitions shown in Table II were derived by best-fits of the residual spectra to Gaussian lines at fixed E_a's and resolutions. No

TABLE II. Summary of the detector efficiencies for Primakoff and Compton conversions on axions of energy E_a, the measured reactor ON-OFF event rates at the signal regions, and the 90% CL upper limits (S_u).

Channel	E_a (keV)	$\epsilon_P(Ge)$	$\epsilon_P(NaI)$	$\epsilon_C(Ge)$	Period I ($\mathrm{day^{-1}\,kg^{-1}}$)	Period III ($\mathrm{day^{-1}\,kg^{-1}}$)	Combined ($\mathrm{day^{-1}\,kg^{-1}}$)	S_u ($\mathrm{day^{-1}\,kg^{-1}}$)
$^{7}Li^{*}$	478	0.36	0.0048	0.61	-0.88 ± 0.75	0.14 ± 0.41	-0.09 ± 0.36	<0.49
$^{135}Xe^{*}$	526	0.34	0.0047	0.58	0.26 ± 0.67	0.38 ± 0.16	0.37 ± 0.15	<0.62
$^{91}Y^{*}$	555	0.33	0.0044	0.58	-0.47 ± 0.67	-0.33 ± 0.15	-0.34 ± 0.15	<0.05
$^{137}Ba^{*}$	662	0.30	0.0040	0.54	-0.46 ± 0.62	-0.02 ± 0.50	-0.19 ± 0.39	<0.46
$^{97}Nb^{*}$	743	0.28	0.0037	0.53	0.14 ± 0.55	0.22 ± 0.37	0.19 ± 0.31	<0.69
$pn \rightarrow d\gamma$	2230	0.16	0.0020	0.37	-0.10 ± 0.17	-0.03 ± 0.03	-0.04 ± 0.03	<0.02

excesses were observed in all channels and upper limits of the signal rates (S_u) at 90% confidence level (CL) were derived. The most sensitive channel in terms of S_u is the 2.23 MeV transition (root-mean-square resolution 2.3 keV) in the $np \rightarrow da$ interaction, because of the lower background level compared to those at ~500 keV (by $\sim 10^{-2}$ [15]).

For completeness, searches were also performed at: (a) half E_a to look for single-γ absorption in $\Gamma_{\gamma\gamma}$ decays, and (b) full E_a of the individual ON/OFF spectra to look for axion emissions from other possible steady-state sources, such as those from the Sun [17,18]. No signals were observed in both cases.

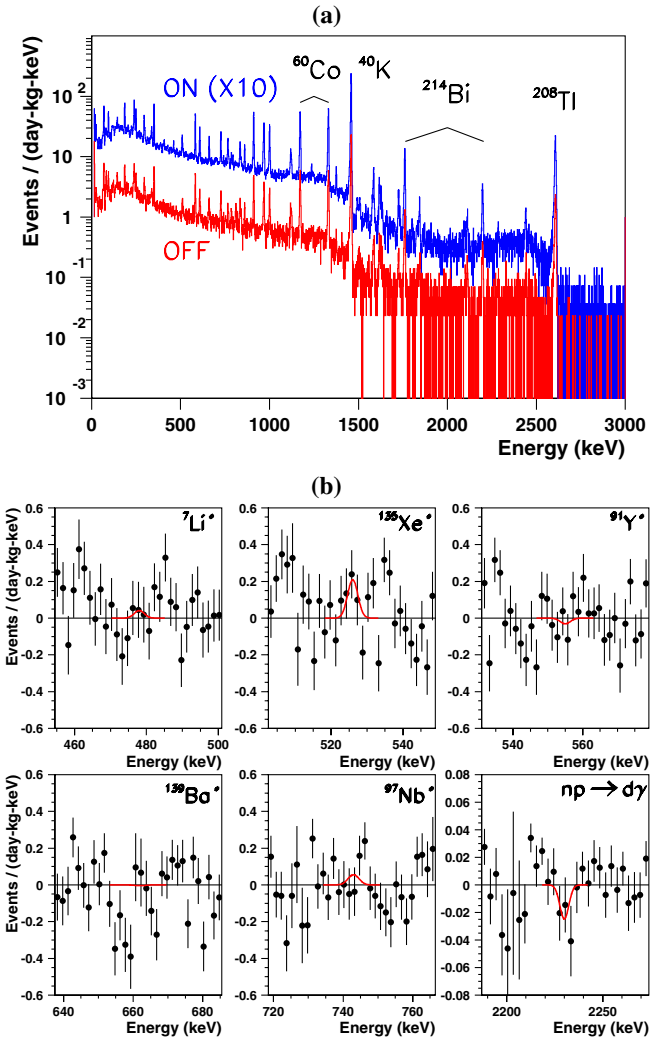

FIG. 4 (color online). (a) The after-cut ON and OFF spectra and (b) the residual spectra for the six specific channels for Period III, with the best-fit Gaussian peaks overlaid.

V. DERIVATIONS OF AXION PARAMETERS

The experimentally measured upper limits S_u of Table II can be translated to bounds among the axion parameters: m_a, $g_{a\gamma\gamma}$, g_{aee}, g^0_{aNN}, and g^1_{aNN}. Two approaches were adopted: (a) specific models were used and tested, and (b) model-independent constraints among the parameters were derived.

A. Branching ratios for axion emissions

The limits S_u are related to reactor axion emission and detection via

$$S_P + S_C < S_u. \tag{14}$$

Both S_P and S_C depend on the reactor axion flux, and thus the branching ratios (Γ_a/Γ_γ).

Starting from the interaction Lagrangian of Eq. (1), the axion emission branching ratio of the $pn \rightarrow d\gamma$ isovector M1 transition can be expressed as [12,19]:

$$\left(\frac{\Gamma_a}{\Gamma_\gamma}\right)_{pn} \equiv \frac{\Gamma_a}{\Gamma_\gamma}(pn \rightarrow d\gamma) = \left(\frac{1}{2\pi\alpha_{\mathrm{em}}}\right)\left(\frac{p_a}{p_\gamma}\right)^3\left(\frac{g^1_{aNN}}{\mu_1}\right)^2, \tag{15}$$

while those for ML transitions in general are [2,12]

$$\frac{\Gamma_a}{\Gamma_\gamma} = \left(\frac{1}{\pi\alpha_{\mathrm{em}}}\right)\left(\frac{1}{1+\delta^2}\right)\left(\frac{L}{L+1}\right)\left(\frac{p_a}{p_\gamma}\right)^{2L+1} \times \left[\frac{g^0_{aNN}\beta + g^1_{aNN}}{(\mu_0 - \frac{1}{2})\beta + (\mu_1 - \eta)}\right]^2. \tag{16}$$

In the formulae, L is the multipolarity of the transition, δ is the known E($L+1$)/ML mixing ratio, and μ_0 and μ_1 are, respectively, the isoscalar and isovector magnetic moments

which can be derived from the proton and neutron magnetic moments (μ_p and μ_n) via:

$$\mu_0 = \mu_p + \mu_n \simeq 0.88 \tag{17}$$

and

$$\mu_1 = \mu_p - \mu_n \simeq 4.71. \tag{18}$$

The nuclear physics of the transitions are parametrized by the matrix elements β and η defined as

$$\beta = \frac{\langle J_f \| \sum_{i=1}^{A} \sigma(i) \| J_i \rangle}{\langle J_f \| \sum_{i=1}^{A} \sigma(i)\tau_3(i) \| J_i \rangle} \tag{19}$$

and

$$\eta = -\frac{\langle J_f \| \sum_{i=1}^{A} l(i)\tau_3(i) \| J_i \rangle}{\langle J_f \| \sum_{i=1}^{A} \sigma(i)\tau_3(i) \| J_i \rangle}, \tag{20}$$

where J_i and J_f are the initial and final nuclear angular momentum in the transitions, while $l(i)$ and $\sigma(i)$ are the orbital angular momentum and nuclear spin operators.

B. Invisible axion models

The evaluations of (Γ_a/Γ_γ) given in Eq. (16) involve modeling of the couplings g^0_{aNN} and g^1_{aNN}. Within the framework of the invisible axion models, these couplings are inversely proportional to the symmetry breaking scale f_a which in turn is related to m_a [7,8] via

$$m_a/\mathrm{eV} = \left(\frac{1.3 \times 10^7}{f_a/\mathrm{GeV}}\right)\left[\frac{\sqrt{z}}{1+z}\right], \tag{21}$$

such that the couplings depend linearly on m_a.

The formulae given in Table 1 of Ref. [7] were adopted for the parametrizations of these axion-nucleon couplings:

$$g^0_{aNN} = C \cdot \left[\frac{(3F-D)}{6}(X_u - X_d - N_f) + \frac{S}{3}(X_u + 2X_d - N_f)\right] \tag{22}$$

and

$$g^1_{aNN} = C \cdot \frac{(D+F)}{2}\left[X_u - X_d - N_f\left(\frac{1-z}{1+z}\right)\right], \tag{23}$$

where the factor common to both couplings is

$$C = 5.2 \times 10^{-8}\left(\frac{3}{N_f}\right)[m_a/\mathrm{eV}]. \tag{24}$$

The terms $D \simeq 0.77$ and $F \simeq 0.48$ [18] are the reduced matrix elements for the octet axial vector currents, $S = 0.33 \pm 0.04$ [20] denotes the flavor singlet axial charge, $N_f = 3$ is the number of families, $z = (m_u/m_d) \simeq 0.56$ is the ratio of the up-to-down quark mass, while X_u and X_d represent, respectively, the PQ charge of the u and d quarks. The KSVZ and DFSZ models differ essentially in their choices of (X_u, X_d).

Previous evaluations of axion fluxes in the stellar [21] and solar [17,18] environment adopted the KSVZ model where $X_u = X_d = 0$. This model also specifies $g_{aee} = 0$ at tree level such that the results are only applicable to probe the axion-photon $g_{a\gamma\gamma}$-couplings. We extended the analysis to include also the DFSZ model, which allows finite $g_{a\gamma\gamma}$-couplings and g_{aee}-couplings. The parameters X_u and X_d are positive-definite constrained by $X_u + X_d = 1$. The values of $X_u = X_d = 0.5$ were chosen for this analysis. Defining

$$g^{0/1}_{aNN} \equiv A^{0/1}[m_a/\mathrm{eV}], \tag{25}$$

the calculable numerical factors $A^{0/1}$ under both KSVZ and DFSZ models are tabulated in Table III. The isovector couplings g^1_{aNN} are the same for both models with this specific choice of (X_u, X_d).

Once g^0_{aNN} and g^1_{aNN} are fixed by the invisible axion models, the evaluations of (Γ_a/Γ_γ) depend on the nuclear physics inputs: δ, β, and η. The values adopted for these parameters are summarized in Table IV. Among the transitions, the $\mathrm{pn} \rightarrow \mathrm{d}\gamma$ is a pure isovector M1 process. Its branching ratio $(\Gamma_a/\Gamma_\gamma)_{pn}$, as given by Eq. (15), is independent of (δ, β, η) and was used in previous reactor axion experiments [10–12]. The $^7\mathrm{Li}^*$ transition is also predominantly M1. The neutron shell is closed and the transition is driven by the odd proton, such that $(\delta, \beta, \eta) \simeq (0, 1, 0.5)$ was adopted as in Ref. [17]. There were no calculations on (β, η) for the remaining four fission daughter isotopes. To make estimations, we project from the results on other heavy isotopes [2,21], also summarized in Table IV. The matrix elements (β, η) for heavy isotopes with unpaired proton and neutron are taken to be $\simeq (1, -3)$ and $\simeq (-1, 1)$, respectively.

Once these (β, η) assignments are made, the branching ratios (Γ_a/Γ_γ) can be readily evaluated with Eqs. (15)–(25). In particular, $\beta \leq 0$ for the odd-neutron nuclei $^{135}\mathrm{Xe}^*$ and $^{137}\mathrm{Ba}^*$, such that the g^0_{aNN} and g^1_{aNN} terms have opposite signs and (Γ_a/Γ_γ) can be vanishingly small within the large nuclear physics uncertainties. These two channels were discarded in subsequent analysis. The variations of (Γ_a/Γ_γ) with m_a of the four remaining channels are depicted in Fig. 5. The differences within the channels and between the KSVZ and DFSZ models are small rela-

TABLE III. The calculated numerical factors $A^{0/1}$ of Eq. (25) under the KSVZ and DFSZ invisible axion models using the formulae of Ref. [7].

Model	I	A^I	Validity
KSVZ	0	-3.5×10^{-8}	{finite $g_{a\gamma\gamma}$, $g_{aee} = 0$} }
$X_u = X_d = 0$	1	-2.8×10^{-8}	
DFSZ	0	-2.6×10^{-8}	{finite $g_{a\gamma\gamma}$ and $g_{aee} = 0$}
$X_u = X_d = 0.5$	1	-2.8×10^{-8}	

TABLE IV. A summary of the nuclear physics input in the evaluations of (Γ_a/Γ_γ). Calculated values of (β, η) on the other isotopes from previous works are included for comparisons. The branching ratios (Γ_a/Γ_γ) at $m_a = 1$ eV under the KSVZ and DFSZ invisible axion models and the QFs relative to that for the pn $\rightarrow$ dγ channel are also shown.

Channel	Unpaired p/n	Transition	δ	β	η	Remarks	$(\Gamma_a/\Gamma_\gamma)^a$ KSVZ model	QF/(QF)$_{pn}$ KSVZ model	$(\Gamma_a/\Gamma_\gamma)^a$ DFSZ model	QF/(QF)$_{pn}$ DFSZ model
pn $\rightarrow$ dγ	—	M1	—	—	—	Refs. [10–12]	7.4×10^{-16}	1.00	7.4×10^{-16}	1.00
^{7}Li*	p	M1	0	1	0.5	Ref. [17]	4.0×10^{-15}	0.50	3.0×10^{-15}	0.43
^{91}Y*	p	M4	0	1	−3	Inferred from Refs. [2,21]	2.1×10^{-15}	0.33	1.5×10^{-15}	0.28
^{97}Nb*	p	M4	0	1	−3		2.1×10^{-15}	0.13	1.5×10^{-15}	0.11
^{135}Xe*	n	M4	0	−1	1		1.6×10^{-16}	0.02	7.1×10^{-18}	0.004
^{137}Ba*	n	M4	0	−1	1		1.6×10^{-16}	0.01	7.1×10^{-18}	0.003
^{65}Cu*	p	M1	0.44	1.81	−6.59	Ref. [2]	1.0×10^{-15}	—	7.1×10^{-16}	—
^{57}Fe*	n	M1	0.002	−1.19	0.80	Ref. [21]	3.4×10^{-16}	—	2.2×10^{-17}	—
^{55}Mn*	p	M1	0.052	0.79	−3.74	Ref. [21]	8.5×10^{-16}	—	6.6×10^{-16}	—
^{23}Na*	p	M1	0.058	0.88	−1.20	Ref. [21]	1.9×10^{-15}	—	1.4×10^{-15}	—

[a]Evaluated at $m_a = 1$ eV.

tive to the scale in the log-log plot, and are represented by the width of the line.

The experimental sensitivities in $g_{a\gamma\gamma}$ and g_{aee} can be described by a quality factor (QF) which is related to the γ-flux Φ_γ of Table I and the upper limit signal rates S_u of Table II via:

$$\frac{1}{g_{a\gamma\gamma/aee}} \propto \mathrm{QF} \equiv \sqrt{\frac{\Phi_\gamma \cdot (\Gamma_a/\Gamma_\gamma)}{S_u}}. \tag{26}$$

Both (Γ_a/Γ_γ) and the relative QF (with respect to that of the pn $\rightarrow$ dγ channel) evaluated at $m_a = 1$ eV were shown in Table IV to illustrate the relative strength of the various channels. It can be seen that the leading contribution to the sensitivities is from the pn $\rightarrow$ dγ channel.

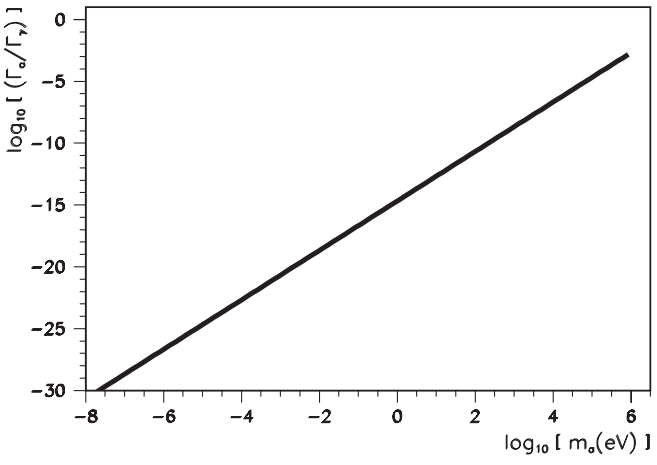

FIG. 5. The variations of (Γ_a/Γ_γ) with m_a in both KSVZ and DFSZ invisible axion models as parametrized in Ref. [7]. The ^{135}Xe* and ^{137}Ba* channels have large uncertainties and were discarded. The width represents the variations within the four remaining channels and among the two models.

C. Model-dependent limits

The (Γ_a/Γ_γ) estimates in Table IV for pn $\rightarrow$ dγ and ^{7}Li* are accurate while those for the four heavy fission isotopes are expected to have large uncertainties. In addition, the relative QF values of Table IV indicate that the pn $\rightarrow$ dγ channel mostly defines the sensitivities. Accordingly, we take the conservative approach that the experimental limits on $g_{a\gamma\gamma}$ and g_{aee} were derived only from this channel. The two detection channels were treated independently, via the relations

$$S_P < S_u \quad \text{and} \quad S_C < S_u, \tag{27}$$

assuming, respectively, $g_{aee} = 0$ and $g_{a\gamma\gamma} = 0$. These produce less stringent bounds compared to those from the convoluted case of Eq. (14), such that the results have general validity.

The exclusion plot of $g_{a\gamma\gamma}$ versus m_a is depicted in Fig. 6. The model-dependence was introduced by fixing $(\Gamma_a/\Gamma_\gamma)_{pn}$ as a function of m_a via Eqs. (15) and (25). The values of $(\Gamma_a/\Gamma_\gamma)_{pn}$ depend only on g^1_{aNN} and are therefore the same for both KSVZ and DFSZ models, as shown in Table IV. Consequently, both models produce a common exclusion region, denoted by "KS." On the other hand, the KSVZ model specifies $g_{aee} = 0$ at tree level, such that only the DFSZ model can be meaningfully applied to define the exclusion region, also labeled as KS, in the g_{aee} versus m_a plot of Fig. 7.

In both Figs. 6 and 7, the vertical bounds labeled "Kine" at 2.23 MeV are due to the kinematical constraints from the maximum E_a. The sensitivities are suppressed at "Decay" for the large $(m_a, g_{a\gamma\gamma}/g_{aee})$ regions, due to $\Gamma_{\gamma\gamma}$ and Γ_{ee} decays in flight. The lack of sensitivities at "Int" for large $g_{a\gamma\gamma} \gtrsim 20$ GeV^{-1} and $g_{aee} \gtrsim 0.2$ are due to axion interactions in the matter between reactor core and detector. Limits marked "R" and "Zn" are, respectively, from previous reactor experiments studying $\Gamma_{\gamma\gamma}$ [10] or Γ_{ee}

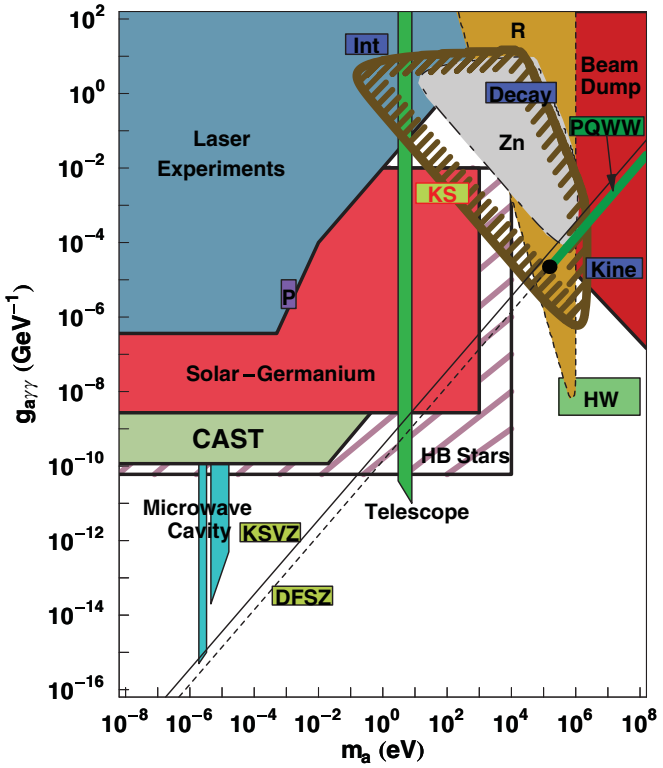

FIG. 6 (color). Exclusion plots of $g_{a\gamma\gamma}$ versus m_a for $g_{aee} = 0$. The limits from the KS experiment at 90% CL are denoted by KS. They are derived by fixing $(\Gamma_a/\Gamma_\gamma)_{pn}$ with the KSVZ and DFSZ invisible axion models. Predicted regions of the PQWW, KSVZ, DFSZ, and HW models on the $(m_a, g_{a\gamma\gamma})$ plane are overlaid. The boundaries defined by Int, Decay, and Kine are constraints due to axions interactions with matter, decays in flights, and kinematics, respectively. The bounds marked Zn are results from Ref. [2], while the region labeled R are from previous reactor axion experiments studying $\Gamma_{\gamma\gamma}$ [10]. Results from the other axion experiments using different techniques [23–26,29] are displayed as colored blocks. The astrophysical bounds [9] are denoted by the striped region.

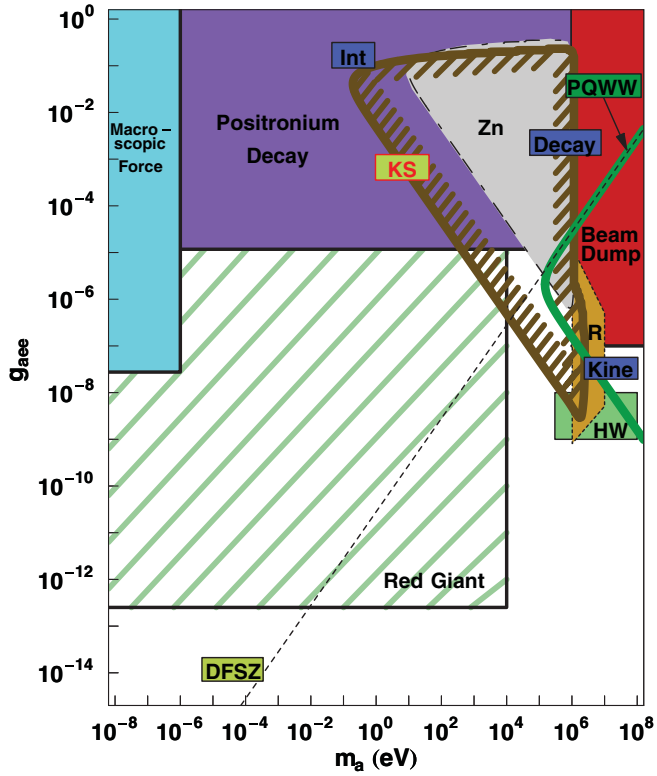

FIG. 7 (color). Exclusion plots of g_{aee} versus m_a for $g_{a\gamma\gamma} = 0$. Similar conventions as in Fig. 6 are adopted. The KS bounds are derived by fixing $(\Gamma_a/\Gamma_\gamma)_{pn}$ with the DFSZ model. The region marked R was excluded by experiment studying Γ_{ee} at reactors [11]. Bounds from other experiments [23,27,28] are shown as colored blocks.

[11] and the radioactive source experiment [2]. They were derived using the same modeling schemes on (Γ_a/Γ_γ) as KS. The bounds from the KS reactor axion searches improve on those of Ref. [2] by 2 orders of magnitude, owing to enhanced axion flux, lower background, and larger data sample.

The KS results define the global exclusion boundaries in $g_{a\gamma\gamma}$ for 10^3 eV $\lesssim m_a \lesssim 10^6$ eV and in g_{aee} for 10^2 eV $\lesssim m_a \lesssim 10^6$ eV. Astrophysics arguments on stellar cooling and red giant yields [1,9] provide more stringent bounds for $m_a \lesssim 10^4$ eV but these are model dependent. They are represented by the striped regions in Figs. 6 and 7, respectively. Comparisons of the KS excluded regions with the KSVZ/DFSZ predictions on the $(m_a, g_{a\gamma\gamma}/g_{aee})$ planes would rule out these models at 10^4 eV $\lesssim m_a \lesssim 10^6$ eV. An example of another existing model predicting axion mass at the MeV range is the HW model [22], also depicted in the figures.

The experimental approach presented in this article can probe the keV-MeV axion mass range which is not accessible to the other techniques. At large $m_a \gtrsim 10^6$ eV, the sensitivities in both $g_{a\gamma\gamma}$ and g_{aee} are dominated by the accelerator-based "beam dump" experiments [23]. Exclusion boundaries at small m_a are defined by: (a) for $g_{a\gamma\gamma}$—the germanium [24] and CAST [25] experiments studying solar axions, and the axion dark matter searches with microwave cavity [26]; and (b) for g_{aee}—the positronium decay [27] and macroscopic force [28] experiments. At $g_{a\gamma\gamma} > 10^{-2}$ GeV^{-1}, the solar axion experiments are limited by axion interactions inside the Sun [9]. Part of this large-$g_{a\gamma\gamma}$ region has been rejected by the optical laser experiments [29], while the KS results contribute to probe and exclude a remaining hole at $m_a \sim 10^1$ eV. For completeness, we mention also the recent PVLAS experiment which reported a finite light polarization rotation in vacuum with a transverse magnetic field [30]. This result was interpreted as the region "P" of finite $(m_a, g_{a\gamma\gamma})$ in Fig. 6, well contradicted by many other experiments. This would imply that it may not be appropriate to analyze the PVLAS results using the existing axion models.

D. Model-independent constraints

The KS exclusion regions of Figs. 6 and 7 were evaluated within the framework of the invisible axion models. Alternatively, it is also instructive to derive model-independent constraints among the axion parameters. Following the reasonings of subsection V C, only the results from the pn $\rightarrow$ dγ channel were adopted, and the two couplings $g_{a\gamma\gamma}$ and g_{aee} were treated independently.

The experimental sensitivities are defined by the signal rates $S_{P/C}$ which are proportional to $g^2_{a\gamma\gamma/aee}(\Gamma_a/\Gamma_\gamma)$ and alternatively, via Eq. (15), to $g^2_{a\gamma\gamma/aye}g^1_{aNN}$. The limit on the Primakoff conversion rate $S_P < S_u(\mathrm{pn} \rightarrow \mathrm{d}\gamma)$ gives rise to the model-independent constraints

$$\begin{cases} g^2_{a\gamma\gamma} \cdot \left(\frac{\Gamma_a}{\Gamma_\gamma}\right)_{pn} < 5.9 \times 10^{-17}\ \mathrm{GeV}^{-2} \\ g_{a\gamma\gamma} \cdot g^1_{aNN} < 7.7 \times 10^{-9}\ \mathrm{GeV}^{-1} \end{cases}, \tag{28}$$

which are applicable within the ranges of $m_a \lesssim 10^5$ eV and $g_{a\gamma\gamma} \lesssim 20\ \mathrm{GeV}^{-1}$, bounded by kinematics and axion interactions in flight, respectively. Similarly, the limit on the Compton conversion rate $S_C < S_u(\mathrm{pn} \rightarrow \mathrm{d}\gamma)$ leads to

$$\begin{cases} g^2_{aee} \cdot \left(\frac{\Gamma_a}{\Gamma_\gamma}\right)_{pn} < 1.7 \times 10^{-20} \\ g_{aee} \cdot g^1_{aNN} < 1.3 \times 10^{-10} \end{cases} \tag{29}$$

for $m_a \lesssim 10^6$ eV and $g_{aee} \lesssim 0.2$. The loss of sensitivities in $g_{a\gamma\gamma}$ at $m_a \sim 10^6$ eV can be explained by the reduction of the Primakoff cross section as depicted in Fig. 3. These constraints on $g_{a\gamma\gamma}$ and g_{aee} as functions of g^1_{aNN} and $(\Gamma_a/\Gamma_\gamma)_{pn}$ are illustrated, respectively, in Figs. 8(a) and 8(b). Limits from the most sensitive laboratory experiments are also displayed for comparisons.

The KS limits on $g_{a\gamma\gamma}$ are not as sensitive as those of CAST [25] and the solar-germanium [24] experiments for $m_a \lesssim 10^4$ eV at all branching ratios. On the contrary, the g_{aee} sensitivities exceed those of the positronium decay [27] and macroscopic force [28] experiments. New regions are probed for $m_a \gtrsim 10^{-6}$ eV with $(\Gamma_a/\Gamma_\gamma)_{pn} > 10^{-9}$ and for $m_a \lesssim 10^{-6}$ eV with $(\Gamma_a/\Gamma_\gamma)_{pn} > 10^{-5}$.

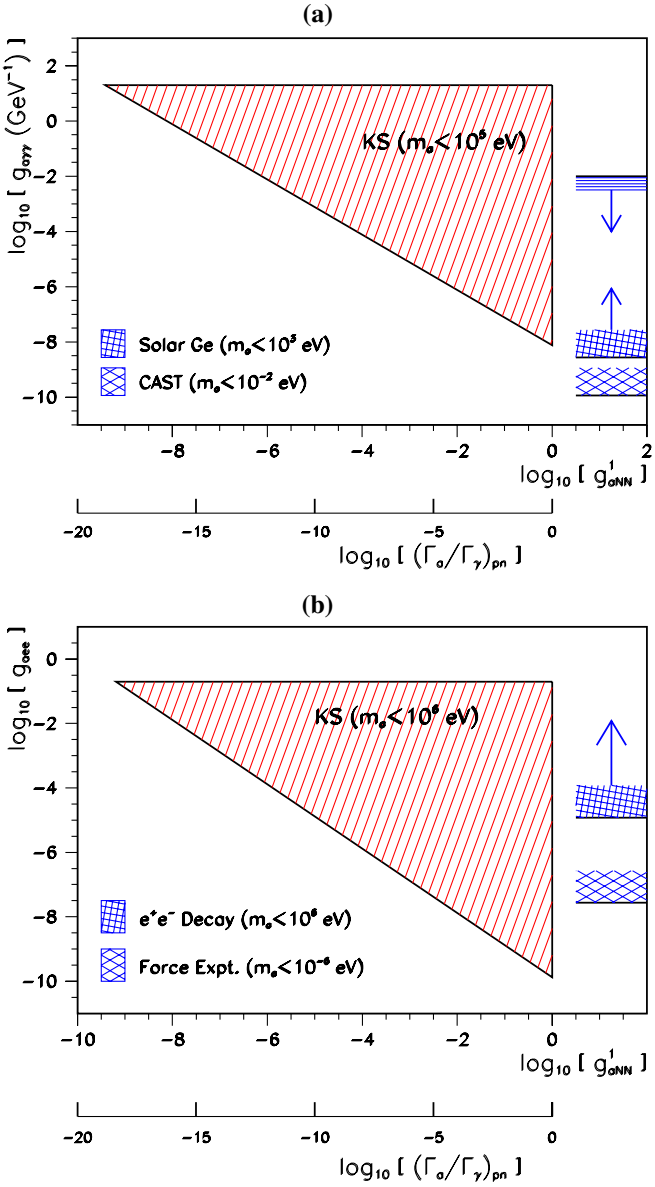

FIG. 8 (color online). The model-independent exclusion regions of the KS experiment for (a) $g_{a\gamma\gamma}$ and (b) g_{aee} on the $(\Gamma_a/\Gamma_\gamma)_{pn}$ and g^1_{aNN} axes. The $g_{a\gamma\gamma}$ and g_{aee} limits from the leading laboratory experiments are also shown for comparisons. The ranges of validity in m_a are indicated.

VI. SUMMARY AND PROSPECTS

This article reports the first study of possible emissions of axions from power reactors using Primakoff and Compton conversions as the detection mechanisms. No evidence was observed and constraints on axion parameters were placed.

The exclusion regions in the $(m_a, g_{a\gamma\gamma}/g_{aee})$ parameter space were identified within the framework of the invisible axion models. The branching ratios for axion emissions associated with radioactive γ-decays are proportional to m_a^2, such that the experiment is sensitive mostly at the large axion mass region. The KS results define the global exclusion boundaries for $g_{a\gamma\gamma}$ and g_{aee} and excluded the KSVZ and DFSZ models for 10^4 eV $\lesssim m_a \lesssim 10^6$ eV.

Independent of models, the KS results are not as sensitive in constraining $g_{a\gamma\gamma}$ compared to those from solar axion searches, but improve on the limits in g_{aee} for branching ratios as small as $(\Gamma_a/\Gamma_\gamma)_{pn} > 10^{-9}$ for light-mass axions such as those within the cosmologically preferred range of 10^{-6} eV $< m_a < 10^{-2}$ eV.

Our studies therefore indicate that this experimental approach can provide competitive sensitivities compared to the other techniques when (a) the axion physics is correctly described by the invisible axion models and the axion mass is at the keV-MeV range, or (b) the axion physics allows relatively large axion-nucleon couplings (and consequently the axion emission branching ratios) at small axion mass not yet covered by the current theoretical modeling.

ACKNOWLEDGMENTS

The authors are grateful for inspiring discussions with Prof. C. Y. Chang, Prof. H. Y. Cheng, Prof. L. Hall, Prof. K. B. Luk, and Prof. K. W. Ng. Suggestions from the referees are warmly appreciated. This work is supported by contracts No. 93-2112-M-001-030, No. 94-2112-M-001-028, and No. 95-2119-M-001-028 from the National Science Council, Taiwan.

[1] See *Review of Particle Physics*, W. M. Yao *et al.*, J. Phys. G **33**, 417 (2006), for details and references.
[2] F. T. Avignone, III *et al.*, Phys. Rev. D **37**, 618 (1988).
[3] R. D. Pecci and H. R. Quinn, Phys. Rev. Lett. **38**, 1440 (1977); Phys. Rev. D **16**, 1791 (1977); S. Weinberg, Phys. Rev. Lett. **40**, 223 (1978); F. Wilczek, Phys. Rev. Lett. **40**, 279 (1978).
[4] D. Kinion, I. G. Irastorza, and K. van Bibber, Nucl. Phys. B, Proc. Suppl. **143**, 417 (2005).
[5] A. R. Zhitnitsky, Sov. J. Nucl. Phys. **31**, 260 (1980); M. Dine, W. Fischler, and M. Srednicki, Phys. Lett. B **104**, 199 (1981).
[6] J. E. Kim, Phys. Rev. Lett. **43**, 103 (1979); M. A. Shifman, A. I. Vainshtein, and V. I. Zakharov, Nucl. Phys. **B166**, 493 (1980).
[7] D. B. Kaplan, Nucl. Phys. **B260**, 215 (1985).
[8] M. Srednicki, Nucl. Phys. **B260**, 689 (1985).
[9] G. G. Raffelt, *Stars as Laboratories for Fundamental Physics* (University of Chicago, Chicago, 1996), Chap. 14; hep-ph/0611350.
[10] J. L. Vuilleumier *et al.*, Phys. Lett. B **101**, 341 (1981); A. Zehnder, K. Gabathuler, and J. L. Vuilleumier, Phys. Lett. B **110**, 419 (1982); V. M. Datar *et al.*, Phys. Lett. B **114**, 63 (1982); G. D. Alekseev *et al.*, JETP Lett. **36**, 116 (1982); J. F. Cavaignac *et al.*, Phys. Lett. B **121**, 193 (1983); V. D. Ananev *et al.*, Sov. J. Nucl. Phys. **41**, 585 (1985); S. N. Ketov *et al.*, JETP Lett. **44**, 146 (1986); H. R. Koch and O. W. B. Schult, Nuovo Cimento Soc. Ital. Fis. A **96**, 182 (1986).
[11] M. Altmann *et al.*, Z. Phys. C **68**, 221 (1995).
[12] T. W. Donnelly *et al.*, Phys. Rev. D **18**, 1607 (1978).
[13] B. Xin *et al.*, Phys. Rev. D **72**, 012006 (2005).
[14] T. R. England and B. F. Rider, Report No. ENDF-349 and No. LA-UR-94-3106, 1993.
[15] H. B. Li *et al.*, Phys. Rev. Lett. **90**, 131802 (2003); H. T. Wong *et al.*, Phys. Rev. D **75**, 012001 (2007).
[16] W. P. Lai *et al.*, Nucl. Instrum. Methods Phys. Res., Sect. A **465**, 550 (2001).
[17] M. Kremar *et al.*, Phys. Rev. D **64**, 115016 (2001); A. V. Derbin *et al.*, JETP Lett. **81**, 365 (2005).
[18] S. Moriyama, Phys. Rev. Lett. **75**, 3222 (1995).
[19] A. Barroso and N. C. Mukhopadhyay, Phys. Rev. C **24**, 2382 (1981).
[20] A. Airapetian *et al.*, Phys. Rev. D **75**, 012007 (2007).
[21] W. C. Haxton and K. Y. Lee, Phys. Rev. Lett. **66**, 2557 (1991).
[22] L. J. Hall and T. Watari, Phys. Rev. D **70**, 115001 (2004).
[23] A. Konaka *et al.*, Phys. Rev. Lett. **57**, 659 (1986); J. D. Bjorken *et al.*, Phys. Rev. D **38**, 3375 (1988); A. Bross *et al.*, Phys. Rev. Lett. **67**, 2942 (1991).
[24] F. T. Avignone, III *et al.*, Phys. Rev. Lett. **81**, 5068 (1998).
[25] K. Zioutas *et al.*, Phys. Rev. Lett. **94**, 121301 (2005).
[26] R. Bradley *et al.*, Rev. Mod. Phys. **75**, 777 (2003).
[27] S. Asai *et al.*, Phys. Rev. Lett. **66**, 2440 (1991).
[28] J. E. Moody and F. Wilczek, Phys. Rev. D **30**, 130 (1984); V. F. Bobrakov *et al.*, JETP Lett. **53**, 294 (1991).
[29] R. Cameron *et al.*, Phys. Rev. D **47**, 3707 (1993).
[30] E. Zavattini *et al.*, Phys. Rev. Lett. **96**, 110406 (2006); A. Ringwald, J. Phys.: Conf. Ser. **39**, 197 (2006).